Velocity Measurement Technique for Permanent Magnet Synchronous Motors Through External Stray Magnetic Field Sensing

Xuyang Liu, *Student Member, IEEE*, Chunhua Liu, *Senior Member, IEEE*, and Philip W. T. Pong, *Senior Member, IEEE*

***Abstract*— This paper presents a technique to measure the velocity of permanent magnet synchronous motors (PMSMs) by sensing the external stray magnetic field outside the stator yoke. A magnetic- equivalent circuit model for the surface-mounted PMSM was developed to analyze the behavior of the stray magnetic field. The external stray magnetic field can provide the position and the speed information of motor rotor. Simulation by means of a 3-D finite-element-method modeling and experimental results over a wide speed range are presented to substantiate the successful application of the proposed technique. A sensitive triaxial tunneling magnetoresistive sensor was employed to measure the stray magnetic field outside the motor stator yoke. The proposed method was validated in both steady and transient operating conditions, and it demonstrated small measurement errors in the range between −0.17% and 0.55% over the speed range from 50 to 1000 rpm. Therefore, it verifies that the proposed technique can provide an easy-to-operate, low-cost, and high-accuracy alternative to the velocity measurement for PMSMs.**

***Index Terms*— Velocity measurement, permanent magnet synchronous motor (PMSM), magnetic equivalent circuit, stray magnetic field, tunnelling magnetoresistive (TMR) sensors.**

I. Introduction

PERMANENT magnet synchronous motors (PMSMs) are currently being widely applied in various industrial applications such as electric vehicles, robotics, wind turbine, etc [1]–[3], mainly because of their superior characteristics of high efficiency, high power density, and high torque-to-current ratio. In these applications, velocity information is one of the most essential parameters for the motor system control and early diagnostic purposes [4], [5]. The variable speed drives for PMSMs primarily rely on the precise velocity and position measurement. Moreover, fault detection and early diagnosis of the motors also require the information of rotation speed. Therefore, a cost-effective and reliable velocity measurement technique is highly desired for PMSMs in their large-scale applications.

By reviewing the past work, it is apparent that there already exist different velocity transducers for electric motors, such as Hall-effect sensors, optical shaft encoders, tachometers and variable reluctance (VR) sensors [6]–[8]. A hall-effect sensor embedded inside the motor stator is the most widely employed method since it can provide stable and uniform field-to-voltage signal [9], [10]. However, embedding the Hall-effect sensors into the stator is a stringent process as the air-gap between rotor magnet and stator is typically below 1 mm. To simplify the process of mounting sensors into the stator, Hall-effect sensors can be installed on the non-driving end of motors [11]–[13]. However, this approach requires extra magnets in addition to rotor magnets, resulting in the larger size and higher cost of motors. Optical shaft encoders can offer high resolution (i.e. over 10000 pulses per revolutions) and symmetrical pulses [14]; nevertheless sometimes it is not feasible to mount an encoder to the motor shaft considering the limitation of size and space. Another drawback of optical encoders is that they are susceptible to contamination from dirt, dust and oil, particularly in the harsh operating environment [15]. Noncontact-type tachometers are preferable for speed measurement as they can detect the rotation of the motor shaft in a non-contact way [8], yet they are usually limited by low resolution, calibration drift and noise contaminations [16]. VR sensors are also frequently used to detect the rotation of a metal wheel that passes the point of sensor especially in automotive applications [17], [18], owing to their low-cost and self-generating signal characteristics. However, VR sensors are only suitable for the wheels with teeth, slots or magnetized poles and they suffer from non-uniform output signals with variable strength and phase that depend on the rotation speed [19].

Sensorless speed measurement technique based on back-EMF and current sensing is another category of velocity measurement method for electrical motors [6], [20]–[22]. This technique requires no position sensors but only electrical measurements. Various techniques such as spectral analysis [23], extended Kalman filter [24], adaptive observer [25], and artificial neural network [26] have been developed for sensorless speed measurement. However, these analysis techniques suffer

Manuscript received January 12, 2018; revised March 7, 2018; accepted March 8, 2018. Date of publication March 19, 2018; date of current version April 23, 2018. This work was supported in part by the Seed Funding Program for Basic Research, in part by the Seed Funding Program for Applied Research, in part by the Small Project Funding Program from The University of Hong Kong, ITF Tier 3 funding, under Grant ITS/203/14, Grant ITS/104/13, and Grant ITS/214/14, in part by the RGC-GRF under Grant HKU 17210014 and Grant HKU 17204617, and in part by the University Grants Committee of Hong Kong under Contract AoE/P-04/08. This is an expanded paper from the IEEE SENSORS 2017 Conference. The associate editor coordinating the review of this paper and approving it for publication was Dr. Qiang Wu. *(Corresponding author: Philip W. T. Pong.)*

X. Liu and P. W. T. Pong are with the Department of Electrical and Electronic Engineering, The University of Hong Kong, Hong Kong (e-mail: ppong@eee.hku.hk).

C. Liu is with the School of Energy and Environment, City University of Hong Kong, Hong Kong.

Digital Object Identifier 10.1109/JSEN.2018.2816931

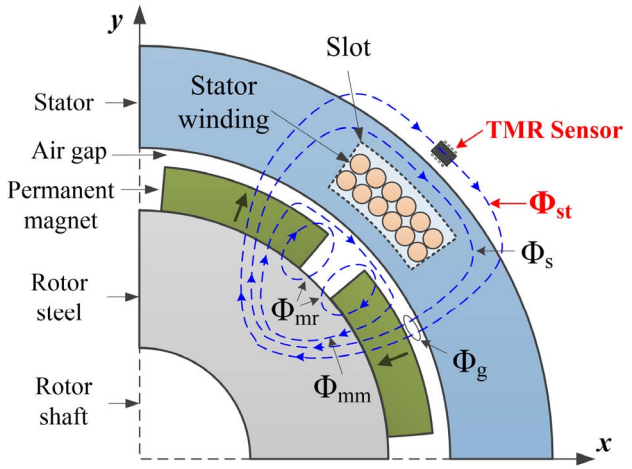

Fig. 1. Cross-section of an 8-pole SPMSM topology and the possible flux paths.

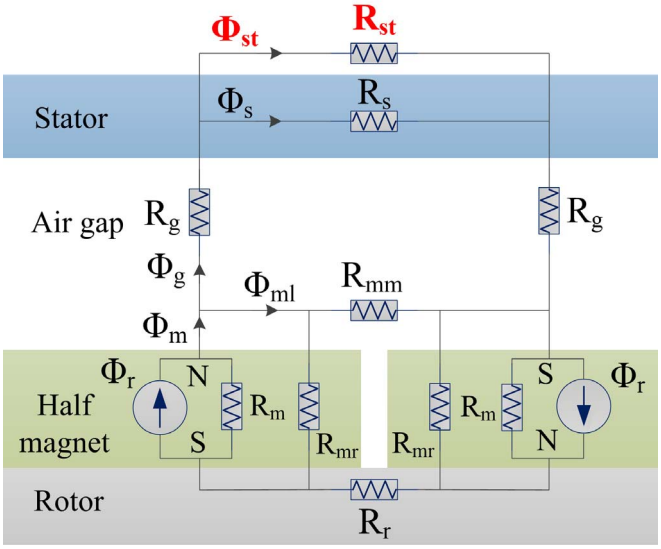

Fig. 2. MEC model for the SPMSM in Fig. 1.

from the drawbacks of long processing time as well as high-cost of the real-time digital signal processors or FPGAs. Hence, these sensorless speed measurement methods are not suitable for the fast speed measurements.

To overcome the abovementioned constraints, a velocity measurement technique for PMSMs by sensing the external stray magnetic field outside the motor stator yoke is proposed in this work [27]. The external stray magnetic field leaking from the stator can give the position and velocity information of the motor rotor. Thus no sensor is required to be installed inside the motor stator in this proposed method. A sensitive tunneling magnetoresistive (TMR) sensor is employed to measure the external stray field in three orthogonal directions, and it can output uniform and symmetric wave signal. A zero-crossing detector (ZCD) is applied to convert the output signal to a square-wave timing signal for speed determination, hence no sophisticated signal processing algorithm is needed.

This paper is organized as follows. Section II provides the fundamental principle of velocity measurement through stray magnetic field sensing. A 3D finite-element-method (FEM) simulation was performed to validate the proposed method in Section III. Section IV shows the experimental implementation of the velocity measurement scheme for PMSMs, whilst Section V presents the experimental results in steady and transient state conditions. Section VI finally addresses the conclusions of this work.

II. Principle of Velocity Measurement Through Stray Field Sensing

In this section, the magnetic equivalent circuit (MEC) method is employed to analyze the behaviour of the external stray magnetic field outside the stator yoke of a surface-mounted permanent magnet synchronous motor (SPMSM). Fig. 1 depicts the cross-section of the simplified motor topology and the flux paths of an 8-pole SPMSM on the *xy* plane. In Fig. 1, the stray leakage flux (Φ_{st}) is part of the main flux that links both stator and rotor but radiates outside the stator yoke. The other flux paths in Fig. 1 are magnet-to-magnet leakage flux (Φ_{mm}), magnet-to-rotor leakage flux (Φ_{mr}), air-gap flux for one magnet pole (Φ_g) and flux through stator core (Φ_s), respectively.

According to the previous research [28]–[31], the stray magnetic flux can be analyzed using a MEC model for the SPMSM structure as depicted in Fig. 2. In this analysis, the stator and rotor steel is assumed to be infinitely permeable everywhere, and the field intensity generated by the armature winding is negligible. In Fig. 2, Φ_r, Φ_m and Φ_{ml} are the flux source of one magnet pole, the flux leaving the magnet and the magnet leakage flux from magnet pole that fails to link stator windings ($\Phi_{ml} \approx \Phi_{mr} + \Phi_{mm}$), respectively. The reluctances shown in Fig. 2 are the reluctance of the magnet (R_m), the reluctance of the air-gap (R_g), the reluctance of rotor core (R_r), the reluctance of stator core (R_s), the reluctance corresponding to Φ_{mm} (R_{mm}), the reluctance corresponding to Φ_{mr} (R_{mr}), and the reluctance corresponding to Φ_{st} (R_{st}), respectively.

To simplify the analysis of the MEC, the magnet-to-magnet leakage flux (Φ_{mm}) and magnet-to-rotor leakage flux (Φ_{mr}) can be eliminated, since they are much lower than the air-gap flux (Φ_g) [28]. The air-gap flux can be expressed as

$$\Phi_g = (1 - k_m)\Phi_m \tag{1}$$

where k_m represents the magnet leakage factor which relates to Φ_{mm} and Φ_{mr} ($k_m < 1$). Hence, Fig. 2 can be simplified to Fig. 3(a) accordingly, then to Fig. 3(b).

In Fig. 3(a), by means of flux division, the air-gap flux can be divided between the stator body and the stray leakage flux path [29], as expressed below:

$$\Phi_{st} = k_{st}\Phi_g = \frac{R_s}{R_s + R_{st}}\Phi_g \tag{2}$$

where k_{st} represents the stray leakage factor which depends on the reluctance values of both R_s and R_{st}.

By adding a reluctance factor (k_r), the reluctance of rotor (R_r) can be eliminated accordingly (see Fig. 3(b)).

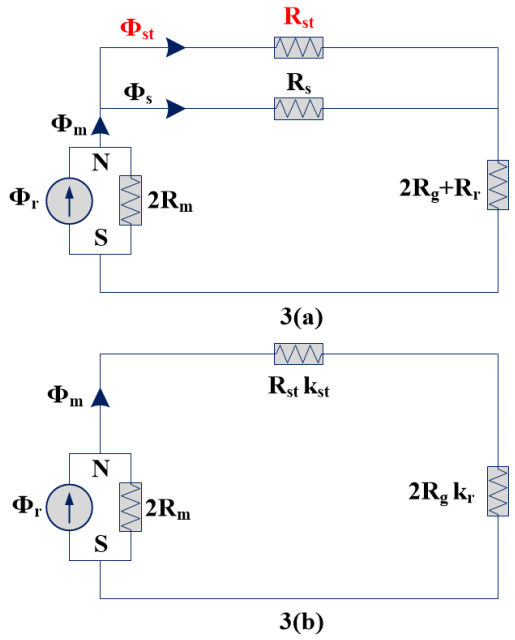

Fig. 3. Simplification of the MEC model in Fig. 2.

Therefore, Φ_m can be calculated as follows:

$$\Phi_m = \frac{2R_m}{2R_m + 2R_g k_r + R_{st} k_{st}} \Phi_r \tag{3}$$

By substituting Eq. 1 and Eq. 3 into Eq. 2, Φ_{st} can be calculated as follows:

$$\Phi_{st} = \frac{2R_m(1-k_m)k_{st}}{2R_m + 2R_g k_r + R_{st} k_r} \Phi_r \tag{4}$$

The reluctances R_g and R_m shown in Fig. 3(b) can be easily obtained as follows [30], [31]:

$$R_g = \frac{g}{\mu_0 A_g} = \frac{g}{\mu_0 (w_m + 2g) l_{st}} \tag{5}$$

$$R_m = \frac{l_m}{\mu_0 \mu_r A_m} = \frac{l_m}{\mu_0 \mu_r w_m l_{st}} \tag{6}$$

In these equations, g is the length of air-gap, l_{st} is the stack length, A_g is the area of air-gap flux, A_g is the area of air-gap flux, w_m is the magnet width, μ_0 is the permeability of the vacuum, and μ_r is the relative permeability of the magnet.

More importantly, the stray leakage reluctance (R_{st}) at one point that is d meters from the stator yoke surface can also be calculated as [29]:

$$R_{stray} = \frac{l_{st}}{\mu_0 A_{st}} = \frac{2d + 2\pi(s + r_s + d)\theta}{\mu_0 (2\pi(s + r_s + d)\theta l_{st})} \tag{7}$$

where l_{st} is the length of the stray leakage reluctance, A_{st} is the area of the stray leakage reluctance, d is the distance between the sensing point and the stator yoke surface, s is the stator thickness, r_s is the radius of stator yoke, and θ is the angle between two adjacent magnet poles.

In terms of magnetic flux density, Eq. 4 can be written as:

$$B_{st} = \frac{2R_m k_m k_{st}}{R_{st}\left(2R_m + 2R_g k_r + R_{st} k_r\right)} B_r \tag{8}$$

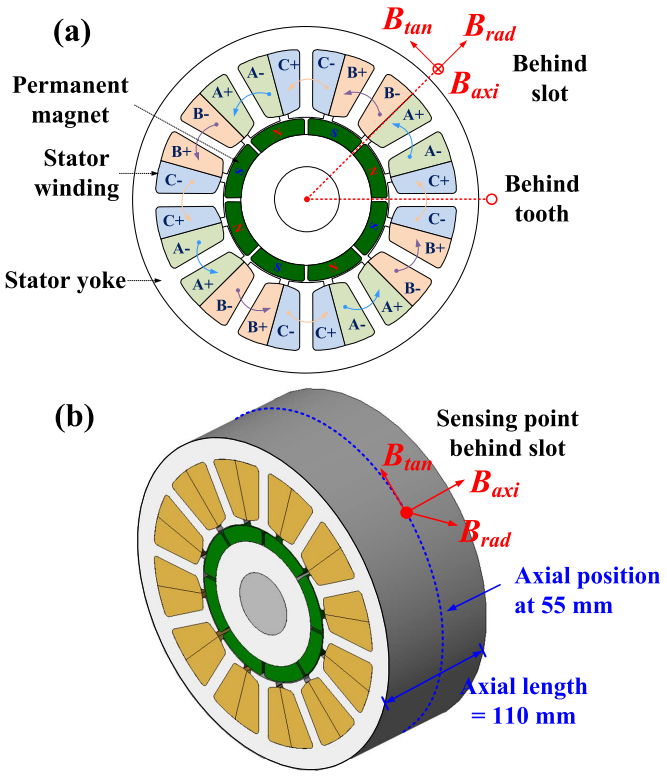

Fig. 4. SPMSM model in simulation. (a) Cross-section view. (b) 3D standard FEM modeling.

TABLE I
MAIN PARAMETERS OF SPMSM MODEL IN SIMULATION

Parameter	Value/type	Unit
Pole/slot	8/12	--
Rated speed	1000	rpm
Rated current	12	A
Axial length	110	mm
Stator outside radius	142.5	mm
Stator inside radius	78	mm
Radius of slot bottom	72.2	mm
Radius of slot top	123.7	mm
Stator slot width	π/12	rad
Outer radius of PM	67	mm
Radius of rotor slot	60.3	mm
Magnet interval	2.8	mm
Permeability of PM	1.32×10^{-6}	H/m
Residual flux density of PM	1.0	T
Material of stator yoke and rotor core	Silicon steel	--
Number of turns per coil	65	--

where B_{st} is the stray leakage flux density, and B_r is the remanence of the permanent magnet (i.e. constant at approximately 1 Tesla). According to Eq. 8, the stray leakage flux density is a function of leakage and reluctance factors, magnetic structure, magnet material and the sensing position.

Therefore, the stray leakage field outside the stator yoke can directly give the position and velocity information of

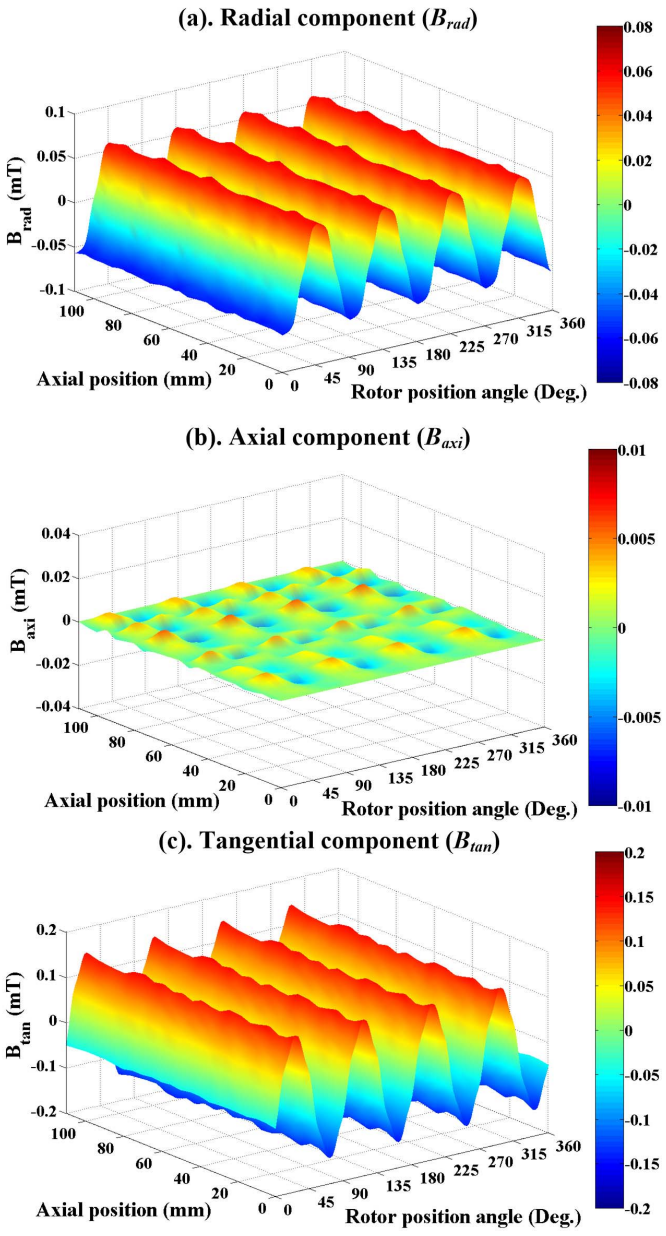

Fig. 5. Simulated stray flux densities at the sensing point that is 2 mm from the stator yoke behind slot.

the magnet poles. When the motor rotor rotates, the stray leakage field also rotates at the same frequency and phase angle. Accordingly, the rotation speed of an SPMSM can be calculated as follow:

$$\omega_m = \frac{60 f_{st}}{p} \text{ (rpm)} \tag{9}$$

where f_{st} is the rotating frequency of the stray leakage field (B_{st}) in Hz and p is the number of magnet pole pairs.

III. FEM Validation

To validate the analytical stray-field model for velocity measurement, an SPMSM model with 8-pole/12-slot was chosen as the test motor, as shown in Fig. 4(a). The test motor with concentrated double-layer winding was fed by a three-phase

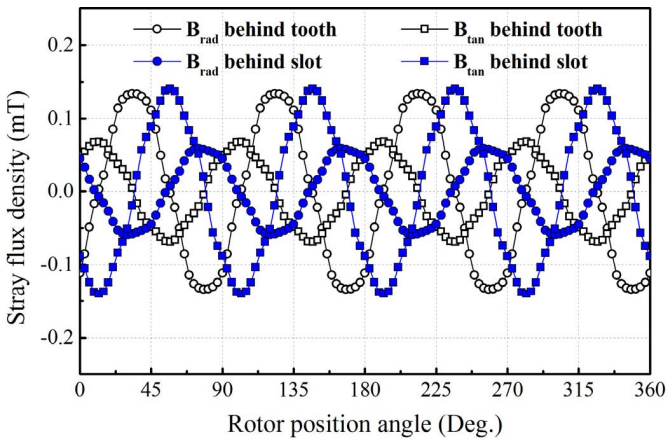

Fig. 6. Simulated stray flux densities at the sensing points behind tooth and behind slot, respectively.

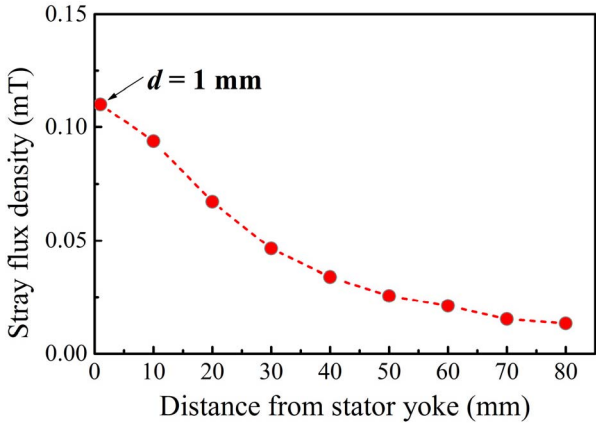

Fig. 7. Simulated stray flux densities versus distance from the stator yoke surface at the middle position of the test motor.

current source in the simulation. The main parameters of the test motor are shown in Table I. The 3-D FEM model of the test motor was simulated by the commercial software JMAG Designer 14 (see Fig. 4(b)).

The radial, tangential and axial field components of stray flux density (i.e. B_{rad}, B_{axi} and B_{tan}) at the sensing point outside the stator yoke that is behind slot and 2 mm from the stator yoke of the test motor are depicted in Fig. 5. The rotation speed of test motor in simulation is 1000 rpm. The result indicates that the amplitudes of the tangential and radial components of stray flux density are much larger than that of the axial component. From Fig. 5(a) and Fig. 5(c), it is apparent that there exists a rotating stray magnetic field (in both radial and tangential directions) outside the stator yoke, which corresponds to the revolution of the motor rotor. B_{rad} and B_{tan} both experience four cycles of stray magnetic flux during each revolution of the rotor shaft (i.e. in 0.06 second), which verify the correctness of velocity calculation through Eq. 9 (i.e. the number of cycles in each revolution equals to the number of magnet pole pairs). Since B_{axi} shows weaker magnetic field signal, it is not used for velocity determination proposes. Moreover, it is preferable to utilize the stray magnetic field near the middle position of the test motor along the axial direction (i.e. axial position

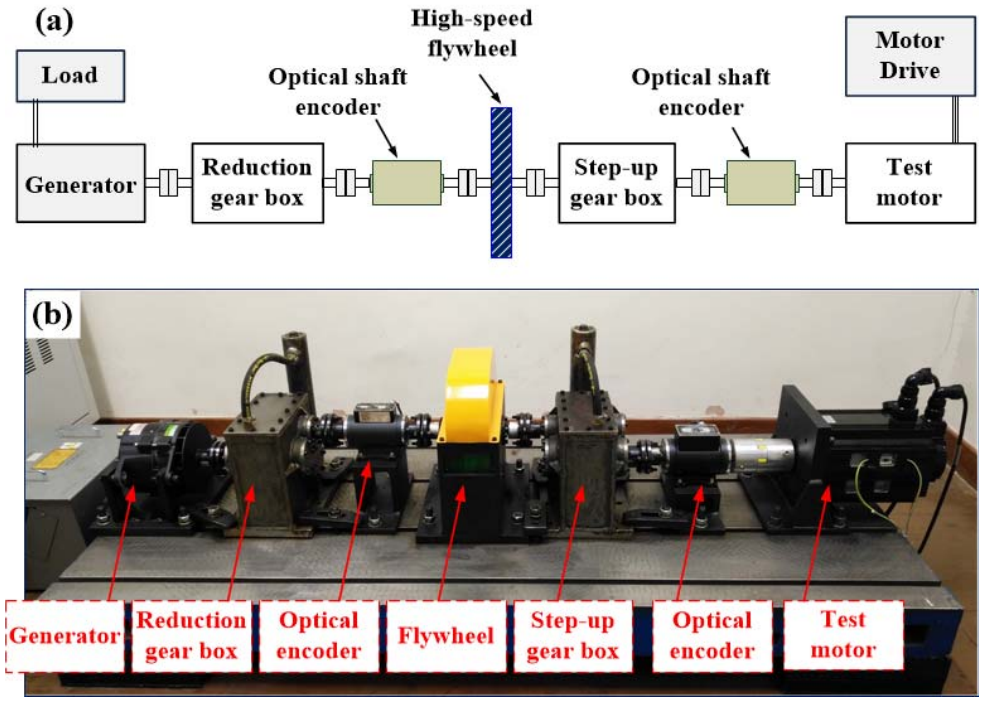

Fig. 8. Schematic (a) and photograph (b) of the testing platform for velocity measurement.

at 55 mm shown in Fig. 4(b)) for velocity measurement purpose.

The shape and amplitude of signal waveforms of stray flux density vary with the sensing position outside the stator yoke. As shown in Fig. 6, the sensing points behind tooth and behind slot both experience four cycles of stray magnetic field in the tangential and radial directions during each revolution of the rotor shaft, but they show different shapes of signal waveforms. The amplitude of B_{tan} behind slot is larger than that of B_{rad} behind slot, whereas the amplitude of B_{tan} behind tooth is lower than that of B_{rad} behind tooth.

The stray leakage reluctance term (R_{st}) increases with the distance from stator yoke surface and the stray leakage flux reduces accordingly as described by Eq. 8. Fig. 7 shows the simulated change in stray flux density values with respect to the distance of the sensing point from the stator yoke surface. It indicates that the stray flux density drops quickly as the distance from the stator yoke surface gets larger due to inverse square law [29]. Hence, it is preferable to mount a magnetic field sensor as close as possible to the stator yoke (i.e. commonly less than 5 mm), so that it can produce larger field-to-voltage output signals and thus better signal-to-noise ratio.

The above simulation results show that the magnitudes of the stray leakage field in the radial, axial and tangential directions are in the order of mT or less, and the frequency of the stray leakage field is typically less than a few kHz. Therefore, it is feasible to mount a tunneling magnetoresistive (TMR) sensor outside the stator yoke to detect the stray leakage field due to its advantages of high sensitivity, large operating range, easy installation and wide dynamic response [32], [33]. A TMR sensor can directly provide the accurate flux density value rather than a relative voltage output that search coil provides. Moreover, the triaxial TMR sensor can provide direction-sensitive outputs in three orthogonal directions. Therefore, the rotation speed of a SPMSM can be easily estimated by the measured stray leakage field outside the stator yoke using a TMR sensor.

IV. Implementation of Velocity Measurement Scheme

A. Testing Platform

To experimentally validate the proposed velocity measurement technique, a testing platform was built in the laboratory. A schematic of the testing platform is shown in Fig. 8(a). A 5.5 kW 8-pole/12-sole SPMSM was installed on the testing platform as the test motor. This three-phase star-connected SPMSM was controlled through space vector control using an adjustable-speed motor drive. The reference rotation speed of the test motor was captured by a precise optical shaft encoder mounted on the motor shaft. The motor was also coupled with a high-speed flywheel and a generator to adjust the load level (see Fig. 8(b)). Meanwhile, the phase currents of the test motor were also monitored by three AC current probes during the experiments.

In order to mount the TMR sensor close to the stator yoke to measure the three-dimensional stray leakage magnetic flux, the motor cover was drilled (four 30 × 30 mm holes as shown in Fig. 9) so that a triaxial TMR TMR2301 sensor could be mounted right outside the stator yoke surface behind slot in the experiment. It should be noticed that the size of the hole can be further reduced (e.g. less than 5 × 5 mm) when designing a new SPMSM. The distance between the TMR sensor and the stator yoke surface is approximately 2 mm.

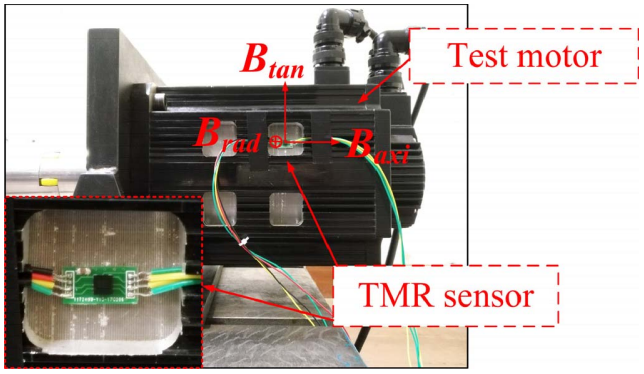

Fig. 9. Triaxial TMR sensor mounted outside the motor stator yoke.

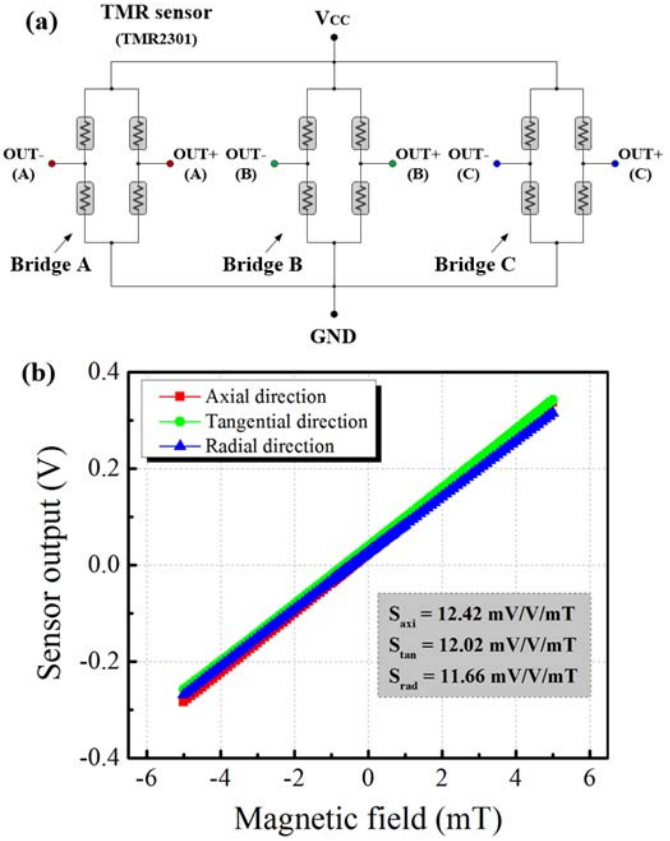

Fig. 10. (a) Layout of the TMR2301 sensor. (b) Typical characteristic curve of TMR sensor at 5V voltage supply.

B. TMR Sensing Technology

The TMR2301 sensor fabricated by the Multi-Dimension Technology (China) is composed of three push-pull Wheatstone bridges, each of which consists of four TMR elements (see Fig. 10(a)), and it requires no set/rest calibration [34]. This sensor operates in a linear magnetic field range of ±5 mT with a typical characteristic output curve shown in Fig. 10(b). The sensitivities of this sensor in three orthogonal sensitive directions are approximately 12 mV/V/mT. This sensor can work in the frequency range up to 1 MHz. Moreover, this sensor is compactly integrated into a 4 mm × 4 mm × 2.5 mm LGA package. Its small size provides flexibility to sense the vector magnetic fields outside the stator yoke.

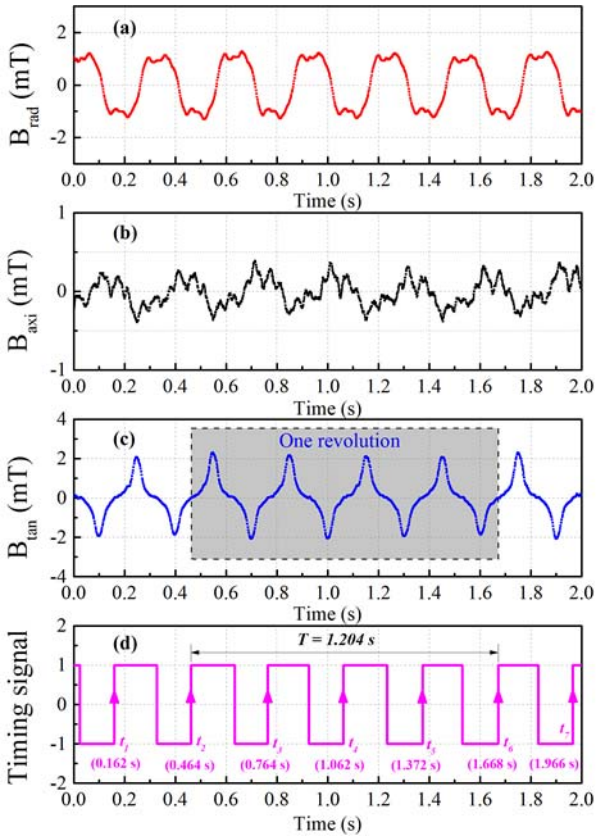

Fig. 11. Rotation speed measurement for the test motor at 50 rpm.

The signal processing unit is composed of the voltage supply, differential amplifier, filter, and A/D converter. The outputs of the sensor were amplified 20 times by the instrumentation amplifiers (AD620) and then filtered by a low-pass filter with cut-off frequency at 1 kHz in order to eliminate the switching noises from motor drive. The output signals were captured by the oscilloscope through the coaxial cable and finally sent to a LabVIEW interface system.

V. Experimental Results and Discussion

A. Steady State Test

The proposed velocity measurement method was firstly validated under steady-state conditions of the test motor. Fig. 10 and Fig. 11 show the measured stray leakage flux density components in tangential, radial and axial directions (i.e. B_{tan}, B_{rad} and B_{axi}) at the velocity of 50 rpm and 1000 rpm, respectively. It shows that the stray leakage field provided relatively stronger flux densities in the tangential and radial directions, which are approximately 2 mT and 1 mT, respectively; whilst the axial component was weaker (i.e. less than 0.5 mT) and more irregular. It can be observed that the signal waveforms of the tangential component at 50 rpm and 1000 rpm were more regular and smoother, and the maxima and minima of the signal of the tangential component remained almost constant. Whereas there exist changes in the waveforms of the radial and axial components from 50 rpm to 1000 rpm, which is caused by the variation of the phase currents and output torques.

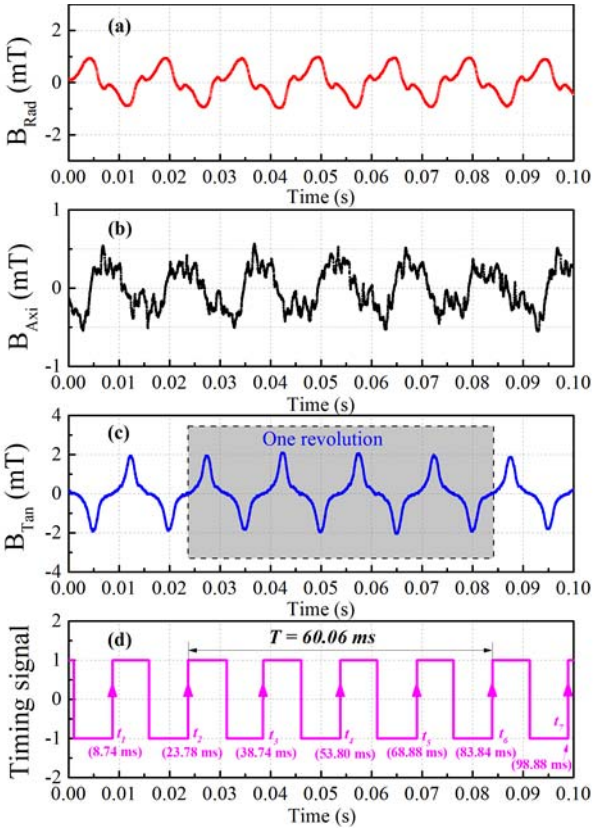

Fig. 12. Rotation speed measurement for the test motor at 1000 rpm.

In Fig. 11(c), each rotor revolution in 1.204 s (i.e. at 50 rpm) generated four cycles of uniform and nearly symmetric signals in the tangential component. Similarly in Fig. 12(c), each rotor revolution in 60.06 ms (i.e. at 1000 rpm) also generated four cycles of signals in the tangential component, which agree well with the pattern of FEM simulation results in Fig. 6. The simulation and experimental results demonstrate that the stray magnetic field that originates from permanent magnet and leaks outside the PMSM (which has a good match with Eq. (8)) can provide the rotational speed of the motor rotor. Although there exists a slight difference between the waveforms of the tangential components from the simulation and experimental results which is due to the minor variation in the motor structure size in simulations and experiments, both results show the same frequency characteristic (i.e. f_{st}) as described in Eq. (9).

As depicted in Fig. 11(d) and Fig. 12(d), a zero-crossing comparison of the signal of the tangential component of the stray leakage field can generate a uniform square-wave timing signal. By detecting the rising edge of the timing signal, the rotation speed of the test motor can be easily determined by

$$\omega_m = \frac{60 f_{st}}{4} = \frac{15}{t_k - t_{k-1}} \text{ (rpm)} \tag{10}$$

where t_k is the time when a rising edge arrives.

Hence, based on Eq. 10, the rotation speeds of the test motor were measured at steady state conditions from 50 rpm to 1000 rpm at an interval of 50 rpm. The measurement results at each steady speed were shown in Fig. 13. It indicates

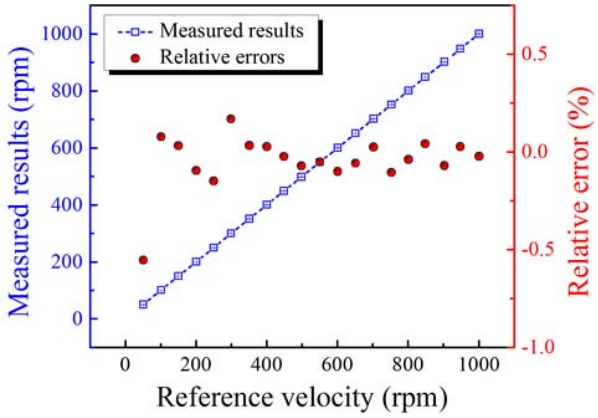

Fig. 13. Measured results at steady state conditions from 50 rpm to 1000 rpm.

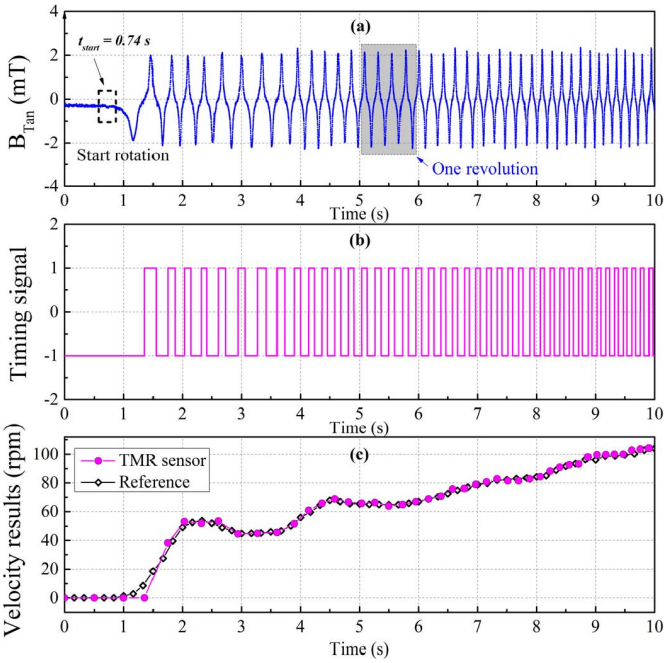

Fig. 14. Measured results at transient state condition from standstill to 100 rpm.

that the proposed technique can provide reliable and stable measurement results at each steady speed and there exists a good linearity between the velocity values measured by the proposed method and the optical shaft encoder in a wide range from 50 rpm to 1000 rpm. The experimental results also demonstrate the high accuracy of the proposed velocity measurement method. The maximum variance under the steady-state conditions was below 2.15 rpm and the relative errors were in the range between -0.17% and 0.55%.

B. Transient State Test

The dynamic performance of the proposed velocity measurement technique under transient state conditions was also investigated and characterized. Fig. 14 shows the velocity measurement results during the starting process of the test motor. The test motor started from standstill to 100 rpm. The tangential component of the stray leakage field started from an initial value and then varied according to the rotation of

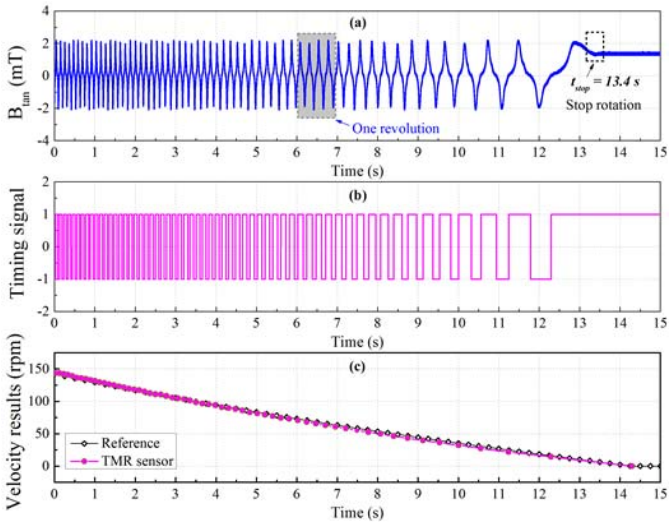

Fig. 15. Measured results at transient state condition from 150 rpm to standstill.

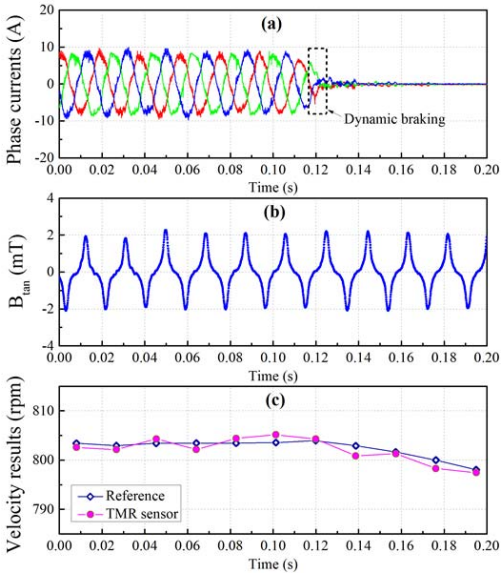

Fig. 16. Measured results under dynamic braking condition.

the motor rotor. The signal in the tangential direction and thus the subsequent square-wave timing signal after zero-cross comparison show an increasing frequency. The velocity values obtained by the proposed technique can match well with the reference velocity measured by the optical shaft encoder (see Fig. 14(c)). The performance of the proposed technique at low speed (e.g. less than 10 rpm) can be easily improved by mounting more than one TMR sensors which are uniformly distributed outside the stator yoke for higher spatial resolution and faster measurement [9].

The sensing performance was also tested for the stopping process. Fig. 15 shows the velocity measurement results during the stopping process of the test motor. The velocity of the test motor decreased from approximately 150 rpm to standstill. The tangential component of the stray leakage field varied according to the rotation of the motor rotor and finally outputted a constant value (Fig. 15(a)). The signal in the tangential direction and thus the consequent square wave after zero-cross comparison show a decreasing frequency accordingly (Fig. 15(b)). The velocity values obtained by the proposed technique match well with the reference velocity obtained by the optical shaft encoder (see Fig. 15(c)).

The proposed technique was also tested well under dynamic braking condition. Fig. 16 shows the velocity measurement results during the process of dynamic braking. The test motor initially rotated constantly at 800 rpm, and then it operated in a dynamic braking mode. The three-phase winding currents become direct, with their angular frequencies equal to zero, as shown in Fig.16(a). Whilst the tangential component of the stray leakage field remained almost unchanged during the dynamic braking phase (see Fig. 16(b)), which proves that the tangential component of the stray field is not affected by the phase currents and it primarily depends on the position of the permanent magnet. The rotation speeds of the test motor were consequently obtained as depicted in Fig. 16(c), and the result matches well with that obtained by the optical shaft encoder. It shows that the proposed technique can work well as the optical shaft encoder when the motor operates in the dynamic braking mode. This characteristic can overcome the constraints of sensorless speed estimation methods that are affected by phase current and back-EMF.

VI. Conclusion

This paper presents a technique for measuring the rotation speed of an SPMSM through sensing the stray leakage magnetic field outside the stator yoke. Both FEM simulation and experimental results are presented to substantiate the successful application of the proposed technique under steady and transient state conditions. A triaxial TMR sensor was mounted outside the stator yoke surface to sense the stray field in three orthogonal directions. It was verified that the tangential component of the stray leakage field can be measured for velocity determination of an SPMSM as it shows the regular and nearly symmetric signal waveform which correlates with the motor rotation. The experimental results show the small measurement errors in the range between -0.17% and 0.55%.

The proposed technique requires no sensors inside the motor stator as compared to the conventional configuration where the Hall-effect sensors are installed inside the motor. The small size of the sensitive TMR sensor allows its easy installation outside the stator yoke surface. It is also worthwhile to highlight that no complicated time-consuming processing algorithm is required in this proposed technique. The square-wave timing signal after zero-crossing detection can be directly applied to obtain the velocity, which is easier and faster to implement than sensorless speed estimation techniques. As such, this technique is promising for velocity measurement application for PMSMs.

References

[1] K. T. Chau, C. C. Chan, and C. Liu, "Overview of permanent-magnet brushless drives for electric and hybrid electric vehicles," *IEEE Trans. Ind. Electron.*, vol. 55, no. 6, pp. 2246–2257, Jun. 2008.

[2] J. Staszak, K. Ludwinek, Z. Gawecki, J. Kurkiewicz, T. Bekier, and M. Jaskiewicz, "Utilization of permanent magnet synchronous motors in industrial robots," in *Proc. Int. Conf. Inf. Digit. Technol.*, Zilina, Slovakia, Jul. 2015, pp. 342–347.

[3] M. E. Haque, M. Negnevitsky, and K. M. Muttaqi, "A novel control strategy for a variable-speed wind turbine with a permanent-magnet synchronous generator," *IEEE Trans. Ind. Appl.*, vol. 46, no. 1, pp. 331–339, Jan./Feb. 2010.
[4] A. Sarikhani and O. A. Mohammed, "Inter-turn fault detection in PM synchronous machines by physics-based back electromotive force estimation," *IEEE Trans. Ind. Electron.*, vol. 60, no. 8, pp. 3472–3484, Aug. 2013.
[5] M. Riera-Guasp, J. A. Antonino-Daviu, and G.-A. Capolino, "Advances in electrical machine, power electronic, and drive condition monitoring and fault detection: State of the art," *IEEE Trans. Ind. Electron.*, vol. 62, no. 3, pp. 1746–1759, Mar. 2015.
[6] J. C. Gamazo-Real, E. Vázquez-Sánchez, and J. Gómez-Gil, "Position and speed control of brushless DC motors using sensorless techniques and application trends," *Sensors*, vol. 10, no. 7, pp. 6901–6947, 2010.
[7] F. Gustafsson, "Rotational speed sensors: Limitations, pre-processing and automotive applications," *IEEE Trans. Instrum. Meas.*, vol. 13, no. 2, pp. 16–23, Apr. 2010.
[8] B. G. Liptak, "7.19 tachometers and angular speed detectors," in *Instrument Engineers' Handbook: Process Measurement and Analysis*, vol. 1, 4th ed. Boca Raton, FL, USA: CRC Press, 2003, pp. 1038–1044.
[9] J. Hu, J. Zou, F. Xu, Y. Li, and Y. Fu, "An improved PMSM rotor position sensor based on linear Hall sensors," *IEEE Trans. Magn.*, vol. 48, no. 11, pp. 3591–3594, Nov. 2012.
[10] S. Y. Kim, C. Choi, K. Lee, and W. Lee, "An improved rotor position estimation with vector-tracking observer in PMSM drives with low-resolution Hall-effect sensors," *IEEE Trans. Ind. Electron.*, vol. 58, no. 9, pp. 4078–4086, Sep. 2011.
[11] P. Yedamale, "Brushless DC (BLDC) motor fundamentals," Microchip Technol. Inc., Tempe, AZ, USA, Appl. Note AN885, Mar. 2003.
[12] "Brushless DC motor control using the LPC2141," NXP Semiconductors, Eindhoven, The Netherlands, Appl. Note AN10661, Oct. 2007.
[13] F. Burger, P.-A. Besse, and R. S. Popovic, "New single chip Hall sensor for three phases brushless motor control," *Sens. Actuators A, Phys.*, vol. 81, no. 1, pp. 320–323, 2000.
[14] D. Mancini, E. Cascone, and P. Schipani, "Galileo high-resolution encoder system," *Proc. SPIE*, vol. 3112, pp. 328–334, Sep. 1997.
[15] H. T. Le, H. Van Hoang, and J. W. Jeon, "Efficient method for correction and interpolation signal of magnetic encoders," in *Proc. 6th IEEE Int. Conf. Ind. Inform.*, Jul. 2008, pp. 1383–1388.
[16] S. J. Arif, M. S. J. Asghar, and A. Imdadullah, "Very fast measurement of low speed of rotating machines using rotating magnetic field," *IEEE Trans. Instrum. Meas.*, vol. 61, no. 3, pp. 759–766, Mar. 2012.
[17] I. Ö. Bucak, "Position error compensation via a variable reluctance sensor applied to a hybrid vehicle electric machine," *Sensors*, vol. 10, no. 3, pp. 1918–1934, 2010.
[18] M. S. Pikula and G. Calves, "Using variable reluctance sensors for differential odometer applications," in *Proc. Vehicle Navigat. Inf. Syst. Conf.*, vol. 2. Oct. 1991, pp. 441–450.
[19] W. J. Fleming, "Overview of automotive sensors," *IEEE Sensors J.*, vol. 1, no. 4, pp. 296–308, Dec. 2001.
[20] M. Aiello, A. Cataliotti, and S. Nuccio, "An induction motor speed measurement method based on current harmonic analysis with the chirp-Z transform," *IEEE Trans. Instrum. Meas.*, vol. 54, no. 5, pp. 1811–1819, Oct. 2005.
[21] Y. Zhao, W. Qiao, and L. Wu, "Improved rotor position and speed estimators for sensorless control of interior permanent-magnet synchronous machines," *IEEE J. Emerg. Sel. Topics Power Electron.*, vol. 2, no. 3, pp. 627–639, Sep. 2014.
[22] R. Kumar, S. Das, P. Syam, and A. K. Chattopadhyay, "Review on model reference adaptive system for sensorless vector control of induction motor drives," *IET Elect. Power Appl.*, vol. 9, no. 7, pp. 496–511, Jul. 2015.
[23] J. M. Aller, T. G. Habetler, R. G. Harley, R. M. Tallam, and S. B. Lee, "Sensorless speed measurement of AC machines using analytic wavelet transform," *IEEE Trans. Ind. Appl.*, vol. 38, no. 5, pp. 1344–1350, Sep./Oct. 2002.
[24] L. Idkhajine, E. Monmasson, and A. Maalouf, "Fully FPGA-based sensorless control for synchronous AC drive using an extended Kalman filter," *IEEE Trans. Ind. Electron.*, vol. 59, no. 10, pp. 3908–3918, Oct. 2012.
[25] A. Piippo, M. Hinkkanen, and J. Luomi, "Analysis of an adaptive observer for sensorless control of interior permanent magnet synchronous motors," *IEEE Trans. Ind. Electron.*, vol. 55, no. 2, pp. 570–576, Feb. 2008.
[26] H. Chaoui and P. Sicard, "Adaptive Lyapunov-based neural network sensorless control of permanent magnet synchronous machines," *Neural Comput. Appl.*, vol. 20, no. 5, pp. 717–727, 2011.
[27] X. Liu, P. W. T. Pong, and C. Liu, "Velocity measurement method for PMSMs through external stray magnetic field sensing," in *Proc. IEEE Sensors Conf.*, Glasgow, U.K., Oct. 2017, pp. 1–3.
[28] T. Goktas, M. Zafarani, K. W. Lee, B. Akin, and T. Sculley, "Comprehensive analysis of magnet defect fault monitoring through leakage flux," *IEEE Trans. Magn.*, vol. 53, no. 4, pp. 1–10, Apr. 2017.
[29] A. A. Adam, K. Gülez, and S. Koroglu, "Stray magnetic field distributed around a PMSM," *Turkish J. Electr. Eng. Comput. Sci.*, vol. 19, no. 1, pp. 119–131, 2011.
[30] H.-K. Yeo, D.-K. Lim, D.-K. Woo, J.-S. Ro, and H.-K. Jung, "Magnetic equivalent circuit model considering overhang structure of a surface-mounted permanent-magnet motor," *IEEE Trans. Magn.*, vol. 51, no. 3, pp. 1–4, Mar. 2015.
[31] R. Qu and T. A. Lipo, "Analysis and modeling of air-gap and zigzag leakage fluxes in a surface-mounted permanent-magnet machine," *IEEE Trans. Ind. Appl.*, vol. 40, no. 1, pp. 121–127, Jan./Feb. 2004.
[32] L. Jogschies *et al.*, "Recent developments of magnetoresistive sensors for industrial applications," *Sensors*, vol. 15, no. 11, pp. 28665–28689, 2015.
[33] R. Weiss, R. Mattheis, and G. Reiss, "Advanced giant magnetoresistance technology for measurement applications," *Meas. Sci. Technol.*, vol. 24, no. 8, p. 082001, 2013.
[34] *TMR2301 3 Axis TMR Linear Sensor Datasheet*. Accessed: Dec. 2017. [Online]. Available: http://www.dowaytech.com/en/1877.html

Xuyang Liu (S'16) received the B.Eng. degree from the University of Electronic Science and Technology of China, Chengdu, China, in 2015. He is currently pursuing the Ph.D. degree with the Department of Electrical and Electronic Engineering, The University of Hong Kong, Hong Kong. His current research interests include nondestructive testing, advanced sensing technologies, and applications of magnetoresistive magnetic field sensors in electric vehicles and wireless power transfer.

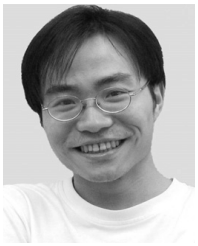

Chunhua Liu (M'10–SM'14) received the B.Eng. and M.Eng. degrees from the Department of Automatic Control, Beijing Institute of Technology, China, in 2002 and 2005, respectively, and the Ph.D. degree from the Department of Electrical and Electronic Engineering, The University of Hong Kong, Hong Kong, in 2009. He is currently an Assistant Professor with the School of Energy and Environment, City University of Hong Kong, Hong Kong.

His research interests are in electrical energy and power technology, including electric machines and drives, electric vehicles, electric robotics and ships, renewable energy and microgrid, and wireless power transfer. In these areas, he has published over 130 refereed papers.

Philip W. T. Pong (SM'13) received the Ph.D. degree in engineering from the University of Cambridge in 2005. He was a Post-Doctoral Researcher with the Magnetic Materials Group, National Institute of Standards and Technology, for three years. In 2008, he joined The University of Hong Kong (HKU) as a member of the Engineering Faculty, where he is now an Associate Professor working on magnetoresistive sensors and their application in smart grid and smart living. He is also a Physicist and an Electrical Engineer with the Department of Electrical and Electronic Engineering, HKU, working on magnetoresistive magnetic field sensors and smart grid.